Elsevier Editorial System(tm) for Molecular Immunology
Manuscript Draft

Manuscript Number: MIMM-D-14-00230R1

Title: In vivo tracking and immunological properties of pulsed porcine monocyte-derived dendritic cells

Article Type: Full Length Article

Keywords: pig, DC tracking, MRI, virus-like particles, immunotherapy

Corresponding Author: Dr. maria montoya, Ph.D.

Corresponding Author's Institution: CReSA

First Author: Elisa Crisci, Dr.

Order of Authors: Elisa Crisci, Dr.; Lorenzo Fraile, Dr.; Rosa Novellas; Yvonne Espada, Dr.; Raquel Cabezón; Jorge Martinez, Dr.; Lorena Cordoba; Juan Barcena, Dr.; Daniel Benitez-Ribas, Dr.; maria montoya, Ph.D.

Abstract: Cellular therapies using immune cells and in particular dendritic cells (DCs) are being increasingly applied in clinical trials and vaccines. Their success partially depends on accurate delivery of cells to target organs or migration to lymph nodes. Delivery and subsequent migration of cells to regional lymph nodes is essential for effective stimulation of the immune system. Thus, the design of an optimal DC therapy would be improved by optimizing technologies for monitoring DC trafficking. Magnetic resonance imaging (MRI) represents a powerful tool for non-invasive imaging of DC migration in vivo. Domestic pigs are closely related to humans and represent an excellent animal model for immunological studies. The aim of this study was to investigate the possibility using pigs as models for DC tracking in vivo.
Porcine monocyte derived DC (MoDC) culture with superparamagnetic iron oxide (SPIO) particles was standardized on the basis of SPIO concentration and culture viability. Phenotype, cytokine production and mixed lymphocyte reaction assay confirmed that porcine SPIO-MoDC culture were similar to mock MoDCs and fully functional in vivo. Alike, similar patterns were obtained in human MoDCs. After subcutaneous inoculation in pigs, porcine SPIO-MoDC migration to regional lymph nodes was detected by MRI and confirmed by Perls staining of draining lymph nodes. Moreover, after one dose of virus-like particles-pulsed MoDCs specific local and systemic responses were confirmed using ELISPOT IFN-γ in pigs. In summary, the results in this work showed that after one single subcutaneous dose of pulsed MoDCs, pigs were able to elicit specific local and systemic immune responses. Additionally, the dynamic imaging of MRI-based DC tracking was shown using SPIO particles. This proof-of-principle study shows the potential of using pigs as a suitable animal model to test DC trafficking with the aim of improving cellular therapies.

Abstract

Cellular therapies using immune cells and in particular dendritic cells (DCs) are being increasingly applied in clinical trials and vaccines. Their success partially depends on accurate delivery of cells to target organs or migration to lymph nodes. Delivery and subsequent migration of cells to regional lymph nodes is essential for effective stimulation of the immune system. Thus, the design of an optimal DC therapy would be improved by optimizing technologies for monitoring DC trafficking. Magnetic resonance imaging (MRI) represents a powerful tool for non-invasive imaging of DC migration *in vivo*. Domestic pigs share similarities with humans and represent an excellent animal model for immunological studies. The aim of this study was to investigate the possibility using pigs as models for DC tracking *in vivo*.

Porcine monocyte derived DC (MoDC) culture with superparamagnetic iron oxide (SPIO) particles was standardized on the basis of SPIO concentration and culture viability. Phenotype, cytokine production and mixed lymphocyte reaction assay confirmed that porcine SPIO-MoDC culture were similar to mock MoDCs and fully functional *in vivo*. Alike, similar patterns were obtained in human MoDCs. After subcutaneous inoculation in pigs, porcine SPIO-MoDC migration to regional lymph nodes was detected by MRI and confirmed by Perls staining of draining lymph nodes. Moreover, after one dose of virus-like particles-pulsed MoDCs specific local and systemic responses were confirmed using ELISPOT IFN-γ in pigs. In summary, the results in this work showed that after one single subcutaneous dose of pulsed MoDCs, pigs were able to elicit specific local and systemic immune responses. Additionally, the dynamic imaging of MRI-based DC tracking was shown using SPIO particles. This

proof-of-principle study shows the potential of using pigs as a suitable animal model to test DC trafficking with the aim of improving cellular therapies.

Highlights:

- Human or pig dendritic cells pulsed with superparamagnetic iron oxide particles did not alter their phonotypic and functional properties *in vitro* in the experimental conditions tested in this work.
- After subcutaneous inoculation in pigs, porcine SPIO-MoDC migration to regional lymph nodes was detected by MRI and confirmed by Perls staining of draining lymph nodes.
- Only one dose of virus-like particles-pulsed MoDCs in pigs was able to induce specific local and systemic responses.
- This proof-of-principle study shows the potential of using pigs as a suitable animal model to test DC trafficking with the aim of improving cellular therapies.

In vivo tracking and immunological properties of pulsed porcine monocyte-derived dendritic cells

Elisa Crisci[1], Lorenzo Fraile[2], Rosa Novellas[3], Yvonne Espada[3], Raquel Cabezón[4], Jorge Martínez[5], Lorena Cordoba[1], Juan Bárcena[6], Daniel Benitez-Ribas[7] and María Montoya[1,8*]

[1] Centre de Recerca en Sanitat Animal (CReSA), UAB-IRTA, Campus de la Universitat Autònoma de Barcelona, 08193 Bellaterra (Cerdanyola del Vallès), Spain

[2] Universitat de Lleida, Lleida, Spain

[3] Fundació Hospital Clínic Veterinari, Departament de Medicina i Cirurgia Animals, Universitat Autònoma de Barcelona, 08193 Cerdanyola del Vallès (Barcelona), Spain

[4] Fundació Clínic per la Recerca Biomèdica, Centre Esther Koplowitz, Barcelona, Spain

[5] Departament de Sanitat i Anatomia Animals, Universitat Autònoma de Barcelona, Spain

[6] Centro de Investigación en Sanidad Animal (INIA-CISA), Valdeolmos, 28130 Madrid, Spain

[7] Centro de Investigación Biomédica en Red de Enfermedades Hepáticas y Digestivas (CIBERehd) and Centre Esther Koplowitz. Barcelona. Spain

[8] Institut de Recerca i Tecnologia Agroalimentàries (IRTA), Barcelona, Spain

*Corresponding author: María Montoya

Tel: +34-935814562

Fax: +34-935814490

E-mail: maria.montoya@cresa.uab.es

Abstract

Cellular therapies using immune cells and in particular dendritic cells (DCs) are being increasingly applied in clinical trials and vaccines. Their success partially depends on accurate delivery of cells to target organs or migration to lymph nodes. Delivery and subsequent migration of cells to regional lymph nodes is essential for effective stimulation of the immune system. Thus, the design of an optimal DC therapy would be improved by optimizing technologies for monitoring DC trafficking. Magnetic resonance imaging (MRI) represents a powerful tool for non-invasive imaging of DC migration *in vivo*. Domestic pigs share similarities with humans and represent an excellent animal model for immunological studies. The aim of this study was to investigate the possibility using pigs as models for DC tracking *in vivo*.

Porcine monocyte derived DC (MoDC) culture with superparamagnetic iron oxide (SPIO) particles was standardized on the basis of SPIO concentration and culture viability. Phenotype, cytokine production and mixed lymphocyte reaction assay confirmed that porcine SPIO-MoDC culture were similar to mock MoDCs and fully functional *in vivo*. Alike, similar patterns were obtained in human MoDCs. After subcutaneous inoculation in pigs, porcine SPIO-MoDC migration to regional lymph nodes was detected by MRI and confirmed by Perls staining of draining lymph nodes. Moreover, after one dose of virus-like particles-pulsed MoDCs specific local and systemic responses were confirmed using ELISPOT IFN-γ in pigs. In summary, the results in this work showed that after one single subcutaneous dose of pulsed MoDCs, pigs were able to elicit specific local and systemic immune responses. Additionally, the

dynamic imaging of MRI-based DC tracking was shown using SPIO particles. This proof-of-principle study shows the potential of using pigs as a suitable animal model to test DC trafficking with the aim of improving cellular therapies.

Keywords: pig, DC tracking, MRI, virus-like particles, immunotherapy

Short title: Dendritic cell tracking in pigs

1. Introduction

Immune cell therapies are being increasingly applied as therapeutic approach, predominantly, with the aim of stimulating immune responses against tumours, infectious diseases or to induce tolerance in autoimmunity (Hilkens and Isaacs, 2013). The success of these treatments will partially depend on accurate delivery of cells to target organs. Dendritic cells (DCs) have a crucial role in initiating and driving the immune responses, thus, antigen-loaded DC immunotherapy has been increasingly used in clinical trials (Ardon et al., 2012). Indeed, DCs are an attractive tool for therapeutic manipulation of the immune system and are currently tested for treatment of cancer (Aarntzen et al., 2012; Banchereau and Palucka, 2005; Figdor et al., 2004; Nestle et al., 2005; Randolph et al., 2005; Schuler et al., 2003) or to ameliorate autoimmune diseases (Giannoukakis et al., 2011; Hilkens and Isaacs, 2013). Although the potential of DC therapy was largely demonstrated, vaccination efficiency needs continuous improvement. Factors influencing DC immunogenicity depend on the subset, maturation state, activation stimulus and optimal conditioning. Route, dosage and frequency of DC injections also need to be optimized (Figdor et al., 2004). Their migration from the site of injection to the draining lymph nodes represents a major requirement for their immunogenic function. Effective migration of injected DCs to the secondary lymphoid organs and an appropriate stimulation of the immune system remains an essential step for DC therapy (Baumjohann et al., 2006).

In previous studies in human, *ex vivo* generated DCs have been administered by different routes: intradermally, intranodally, subcutaneously, intravenously, intralymphatically or using combination of these routes (Baumjohann and Lutz, 2006; de Vries et al., 2005; Wilgenhof et al., 2013). Currently, in the case of solid tumors

101 treatment, intradermal or subcutaneous administrations of DCs are most frequently used
102 followed by intravenous and intranodal injection (Verdijk et al., 2009). Nevertheless,
103 the optimal route of administration for each DC therapy is not well established. In
104 addition, the efficiency of DC migration to the lymph nodes is rather low (up to 4% of
105 injected DCs migrate to the draining lymph nodes) (Verdijk et al., 2009). Thus,
106 designing an optimal DC therapy would therefore be facilitated by technologies for
107 monitoring DC trafficking *in vivo* and by efficient monitoring of lymph node homing by
108 a non-invasive method (Baumjohann et al., 2006).
109 Recent development of new methods to follow DC migration by non-invasive imaging
110 modalities such as scintigraphy, PET or magnetic resonance or bioluminescence
111 imaging have gained attraction because of their potential clinical applicability in human
112 (Baumjohann and Lutz, 2006). Magnetic resonance imaging (MRI) of cells labelled
113 with magnetically visible contrast agents after either direct injection or local or
114 intravenous infusion has the potential to fulfil this goal. MRI is well suited as an
115 imaging modality for non-invasive cell tracking because of its tissue characterization,
116 excellent image quality, and high spatial resolution, although nuclear imaging is more
117 sensitive. In general terms, MRI benefits are: lack of ionizing radiation, high spatial
118 resolution, flexible image contrast and the ability to assess regional function, perfusion
119 and necrosis (Rogers et al., 2006). Thus, MRI represents a sophisticated tool for non-
120 invasive imaging of DC migration *in vivo* (Baumjohann and Lutz, 2006).
121 Iron oxide particles are part of a class of superparamagnetic MRI contrast agents. These
122 particles range in size from tens of nanometers in diameter (ultrasmall
123 superparamagnetic iron oxide (USPIO)), to 100 nm (superparamagnetic iron oxide
124 (SPIO)) (Bulte and Kraitchman, 2004; Hoehn et al., 2007; Rogers et al., 2006). The
125 relation of particle size to the rate of endocytosis was shown for *in vitro* human

monocytes by simple incubation of SPIO particles Endorem® (Guerbet, Villepinte, France) (Metz et al., 2004). SPIO phagocytic uptake is mediated by scavenger receptor SR-A (Raynal et al., 2004) and SPIO (Endorem®) show higher uptake rates than smaller particles (20-40) (Baumjohann et al., 2006). DCs are another cell type that can endocytose SPIO labels and can be used in MRI (Rogers et al., 2006). Different studies were performed in mice using MRI-based quantification of antigen presenting cell number in the draining lymph nodes (Baumjohann et al., 2006; Long et al., 2009) and Baumjohann *et al*. has shown that after subcutaneous injection of one million DCs there was still a clear MRI signal detectable in the draining lymph node that also correlated with immunohistological detection (Baumjohann et al., 2006).

Virus-like particles (VLPs) present overall suitable characteristics for their uptake by DCs and subsequent processing and presentation to effector cells of the immune system (Crisci et al., 2012a). VLPs from rabbit hemorrhagic disease virus (RHDV) have shown to be good platforms for inducing immune responses against an inserted foreign epitope in mice (Barcena et al., 2004; Crisci et al., 2009; Luque et al., 2012). Recently, we successfully used chimeric RHDV-VLPs containing a well-known T-cell epitope derived from the 3A protein of foot-and-mouth disease virus (Cubillos et al., 2012) to induce specific T-cell responses in pigs (Crisci et al., 2012b).

Domestic pigs share similarities in physiology, immunology, anatomy and size with humans, and represent an excellent animal model for immunological studies. Indeed, experiments in pigs are much more likely to be predictive of therapeutic treatments in humans than experiments in rodents. An exhaustive recent review (Meurens et al., 2012) highlighted the importance of the pig model for human research and vaccine development. Recently, pigs have been used to investigate the *in vivo* tracking and their

therapeutic effect of autologous mesenchymal stem cells (MSCs) by intracoronary transplantation on myocardial infarction (MI) (Peng et al., 2013).

Considering all these premises, the aim of this study was to investigate the possibility to use conventional pigs as a model for DC tracking *in vivo* by MRI. This study has shown that DCs could be labelled with SPIO particles without affecting their function. Porcine SPIO pulsed MoDCs migration to regional lymph nodes was detected. Additionally, SPIO pulsed MoDCs when incubated with the appropriate antigen (chimeric RHDV-VLPs), were fully functional eliciting local and systemic responses in pigs. This is the first proof-of-principle report describing swine DC tracking *in vivo* and the efficacy of DC-based immunization.

2. Materials and methods

2.1 Porcine monocyte-derived and human monocyte-derived dendritic cell generation

Porcine PBMCs were obtained from clinically healthy Large White X Landrace pigs of eight weeks of age. Porcine monocyte-derived dendritic cells (poMoDCs) where generated by a five-day protocol as previously described by (Carrasco et al., 2001; Silva-Campa et al., 2010). Briefly, freshly isolated PBMCs were placed in tissue culture flasks and incubated overnight at 37 °C in 5% CO_2 to allow monocytes to adhere. Non-adherent cells (peripheral blood lymphocytes, PBLs) were removed by washing with DMEM (Lonza) and frozen for use in mixed lymphocyte reaction (MLR) experiments. Adherent cells were cultured in complete DMEM (culture medium containing 2mM of L-glutamine (Invitrogen®, Barcelona, Spain), 100 U/ml of Polymixin B (Sigma–Aldrich Quimica, S.A., Madrid, Spain), 10% of fetal calf serum (FCS) (Euroclone, Sziano, Italy) and 100 µg/ml of penicillin with 100 U/ml of streptomycin (Invitrogen®,

Barcelona, Spain) containing 40 ng/mL of recombinant porcine GM-CSF (R&D Systems) and 40 ng/mL of recombinant porcine IL-4 (R&D Systems) at 37 °C in 5% CO_2. Cells were incubated for 5-6 days with cytokine-containing medium replacement on day 3. MoDCs were harvested on day 5 or 6 using cell dissociation enzyme-free Hank's-based buffer (Gibco® Cell Dissociation Buffer) and resuspended in complete DMEM. Stimuli were added at day 5 or 6 and mature and immature poMoDCs were analyzed by flow cytometry and cytokine ELISA.

In order to generate human monocyte derived dendritic cells (huMoDCs), PBMCs from healthy donors were allowed to adhere 2 h at 37 ºC. The adherent monocytes were cultured in X-VIVO 15 medium (BioWhittaker, Lonza, Belgium) supplemented with 2% AB human serum (Sigma-Aldrich, Spain), IL-4 (300 U/mL), and GM-CSF (450 U/mL) (Both from Miltenyi Biotec, Madrid, Spain) for 7 days. The present study was approved by the Ethics Committee at the Hospital Clinic of Barcelona. Buffy coats were obtained from Banc de Sang i Teixits and written informed consent was obtained from all blood donors.

2.2 Dendritic cell labelling with SPIO

After 5 days poMoDCs were incubated overnight with SPIO particles (Endorem®, 11.2 mg Fe/mL, Guebert, Aulnay-sous-Bois, France) at different iron concentrations ranging from 25 to 200 µg Fe/mL. Viability of cells was checked by trypan blue staining and by flow cytometry using LIFE/DEAD Fixable Dead Cell Stain Kit (Life Technologies), and FITC-conjugated Annexin V (Caltag Laboratories). Cells were stained during 15 min at 4°C. Flow cytometry was performed using BD FACSCanto II, and data were analyzed with BD FACSDiva 6.1™ software.

SPIO particles were added to huMoDCs at day 5, and huMoDCs phenotype and cytokine production was analysed at day 7 by flow cytometry and ELISA respectively.

The same batch of SPIO particles was used in porcine and human DC studies. Human and porcine moDCs incubated with medium alone and without SPIO and/or stimuli were used as negative control and referred as Mock moDCs in the figures.

2.3 Expression and purification of recombinant RHDV-VLPs

In this study, native RHDV-VLPs and chimeric RHDV-VLPs harbouring a T-cell epitope derived from foot and mouth disease virus 3A protein (RHDV-3A-VLPs) were used, as previously reported (Crisci et al., 2012b). The recombinant VLPs were expressed in H5 insect cell-cultures infected with the corresponding recombinant baculoviruses and purified as previously described (Crisci et al., 2012b).

2.4 Stimulation of poMoDCs and huMoDCs

For *in vitro* studies, poMoDCs and SPIO-poMoDCs were stimulated with RHDV-VLPs (60 µg/mL) and LPS (10 µg/mL) (Lipopolysaccharides from *Escherichia coli* O111:B4, Sigma). Stimuli were plated with both poMoDCs after 6 days of culture ($2.5x10^4$ cells/50 µL/well) in 96-well plates. In SPIO-poMoDCs cultures, stimuli were plated the day after SPIO particles labelling. Before any analysis or inoculation, SPIO particles and stimuli excesses were thoroughly washed away.

To generate mature huMoDCs, a maturation cocktail was added on day 6 for 24 h. This cocktail consisted of IL-1β, IL-6 (both at 1000 IU/mL), TNF-α (500 IU/mL) (CellGenix, Freiburg, Germany) and Prostaglandin E2 (PGE2, 10 µg/mL; Dinoprostona, Pfizer).

224

225 **2.5 Flow cytometry analysis of poMoDCs and huMoDCs**

226 Flow cytometry analysis of poMoDCs was performed using an indirect labelling for
227 CD172a (SIRP-α), SLA-I (MHC-I), SLA-II (MHC-II), CD4, CD11R3 (resemble
228 CD11b), CD80/86 (B7-1/B7-2) and CD163 (scavenger R) and direct labelling for CD14
229 (LPS R) and CD16 (FcγRIII) (reviewed in (Summerfield and McCullough, 2009) and
230 (Ezquerra et al., 2009)). Unless specified below, reagents were derived from hybridoma
231 supernatants. Briefly, poMoDCs were labelled during 1 h at 4ºC for each CD marker,
232 using 30 µl of antibody solution. Anti-CD172a (SWC3, BA1C11), anti-SLAI (4B7/8),
233 anti-SLAII (1F12), anti-CD4 (76-12-4), anti-CD11R3 (2F4/11), CTLA4-mIg (Ancell,
234 Minnesota, USA), anti-CD163 (2A10/11), anti-CD14-FITC (MIL2, Serotec, bioNova
235 cientifica, Madrid, Spain) and anti-CD16-FITC (G7, Serotec) were used. After
236 incubation, they were washed with cold PBS with 2% FCS by centrifugation at 450 g,
237 4ºC for 5 minutes. Then, the secondary antibody R-phycoerythryn anti-mouse IgG
238 (Jackson ImmunoResearch, Suffolk, UK) diluted 1:300 was added when required. Cells
239 were incubated for 1 h at 4ºC, they were washed as before and resuspended in PBS with
240 2% FCS. Stained cells were acquired on Coulter® EPICS XL-MCL cytometer and
241 analysed by EXPO 32 ADC v.1.2 program.

242 To characterize and compare the phenotype of the huMoDC populations the following
243 mAbs or appropriate isotype controls were used: CD80, CD83, CD86 (BD-Biosciences)
244 and FITC-labelled MHC class II (BD-Pharmingen). Primary antibodies were followed
245 by staining with PE-labelled goat-anti-mouse (BD Biosciences). Flow cytometry was
246 performed with FACSCanto II™ and analysed with FACSDiva software (BD
247 Biosciences) and with WinMDI software (version 2.9).

248

2.6 Cytokine ELISAs

Cytokine levels in conditioned cell supernatants were assayed by ELISA for porcine TNF-α and IL-6 at 24 h. For each ELISA, triplicate wells of stimulated- or un-stimulated-cells supernatants were used and all the results were analyzed with KC Junior Program (Bio Tek Instruments, Inc) using the filter Power Wave XS reader. For porcine TNF-α and IL-6 a DuoSet® ELISA Development system (R&D Systems, Abingdon, UK) was used following manufacturer's instructions.

IFN-γ (BD-Biosciences) from human MLR supernatants was analyzed by ELISA for human according to the manufacturer's guidelines.

2.7 Mixed lymphocyte reaction

Mixed lymphocyte reaction (MLR) was evaluated by flow cytometry using the fluorescent dye carboxyfluorescein succinimidyl ester (CFSE; Molecular Probes) for poMoDCs as previously described (Silva-Campa et al., 2010). The optimal conditions for the MLR were determined in preliminary experiments using different stimulator:responder cell ratios and different incubation times. PoMoDCs and SPIO-poMoDCs were cultured with CFSE labelled-PBLs at a ratio 1:20 (MoDCs:PBLs). PoMoDCs and SPIO-poMoDCs were incubated with phytohaemagglutinin (PHA) (20 μg/mL, Sigma) as postivie control or medium as negative control. Cultures were incubated at 37°C in 5% CO_2 for 4 days. The percentage of proliferation was evaluated and values were represented as the mean of triplicate wells and representative of three different experiments, corresponding each one to a different animal.

MLR was also tested for human DCs. Allogeneic T cells were co-cultured with huMoDCs differently generated in a 96-well microplate (in triplicates). For the

proliferation assay, a tritiated thymidine (1 µCi/well, Amersham, UK) was added to the cell cultures on day 6 and an incorporation assay was measured after 16 h.

2.8 *In vivo* experimental designs

At the age of 6-7 weeks, ten male conventional pigs (Large White x Landrace) were selected from a high health status farm located in the Northern part of Spain; these pigs were porcine reproductive and respiratory syndrome virus and porcine circovirus type 2 negative and clinically healthy at the beginning of the experiment. Pigs received non-medicated commercial feed *ad libitum* and had free access to drinking water. Animals were housed in an experimental farm (CEP, Torrelameau, Lleida, Spain) in different pens.

Pigs were identified, ear-tagged and randomly distributed into four groups, namely A (n = 3), B (n = 3), C (n = 2) and D (n = 2) balanced by weight (range 17.5-23 kg). Pigs of group C remained untreated and were used as negative controls. Groups A and B were inoculated once subcutaneously (SC) into right inguinal zone with RHDV-3A-VLP- and RHDV-VLP-pulsed MoDCs respectively. Group D was inoculated once with unpulsed MoDCs. Group A, B and D were inoculated with 1 mL of MoDCs (approx. $5x10^5$ viable cells/mL/pig) 7 days after blood collection. Each pig was inoculated with MoDCs derived from its own PBMCs, since animals were not inbred. Subgroups were organized as summarized in **Table 1**. Pigs were monitored daily for immunisation reactions and samples of blood were collected at day 0 and 21. Fourteen days after the DC immunisation, pigs were euthanized with an intravenous overdose of sodium pentobarbital and blood and superficial inguinal lymph nodes (InLNs) were collected at culling.

297 Additionally, at the age of 4-5 weeks, four female piglets (Large White x Duroc x
298 Pietrain) were divided in 2 groups, E and F (**Table 1**). Two piglets (E) were SC
299 inoculated once into right inguinal zone with SPIO-MoDCs (approx. 5 x 10^5/mL viable
300 labelled DCs) and two additional piglets (F) with RHDV-3A-VLP pulsed SPIO-MoDCs
301 6 days after blood collection. One piglet of group E was used for MRI tracking *in vivo*
302 and group E was sacrificed two days after the MoDC injection. Group F was sacrificed
303 one week after MoDC inoculation. At culling of group E and F blood and InLNs were
304 collected for histological and immunological studies (**Fig. 7 supplementary data**).
305 The experiment received prior approval from the Ethics committee for Animal
306 Experimentation of the Institution (Universitat Autònoma de Barcelona, permit number:
307 1189). The treatment, housing and husbandry conditions conformed to the European
308 Union Guidelines (The Council of the European Communities 1986, EU directive
309 86/609/EEC). All efforts were made to minimize animal suffering.
310
311 **2.9 *In vivo* dendritic cell tracking with MRI**
312 For MRI *in vivo* tracking, a 4-5 week old piglet (approx. 12 kg) was used. PBMCs were
313 collected at D0 and poMoDCs were generated as described above. At day 5 poMoDCs
314 were incubated overnight with SPIO at 50 μg Fe/mL and around 5 x 10^5/mL viable
315 SPIO-MoDCs were injected SC into the right inguinal zone at day 6. MRI of the
316 draining LN regions was acquired under anaesthesia at different times prior and post
317 MoDC injection. The pig was anesthetized with 5 mL of azaperone (Stresnil®) and
318 ketamine (Imalgene®) mixed solution and maintained with isoflurane anesthesia during
319 MRI scans. MRI was performed before inoculation (basal MRI) and after 20 minutes,
320 30 and 46 h post inoculation. The pig was imaged using a 0.18 T magnetic resonance
321 system (Vet-MR, Esaote, Genova, Italy) with a knee coil for signal reception, in dorsal

recumbency. MRI was obtained with a gradient echo pulse sequence; T2*-weighted transverse images were acquired with an echo time of 14 ms, repetition time 410 ms, flip angle 30º, 4.4 mm slice thickness and an average total acquisition time of 7 min and 29 seconds. At 48 h post inoculation the pig was euthanized and InLNs were used for histological studies and Prussian blue staining.

2.10 Staining and immunohistochemistry of histopathological sections

Left and right InLNs were fixed in 10% buffered formalin and routinely processed for histopathology. Sections 3 μm thick were cut, stained with hematoxylin and eosin (H-E) and observed in a blinded-fashion method. Reactivity in each InLN was evaluated by means of a semi-quantitative score taking into account the percentage of secondary follicles in the whole InLN section; the following scoring was used: 0-5% (-), 0-30% (+), 30-70% (++), 70-100% (+++).

Additionally, cell culture or tissue sections were stained with Prussian blue (Perls' staining) to detect SPIO-labeled cells. Briefly, slides were stained with 2% potassium hexacyanoferrate (II)-trihydrate in 0.2 M HCl for 30 min and counterstained with eosin. The amount of positive cells was measured using digital morphometry software (ImageJ). Two sections were analyzed for each lymph node, and for each section, three low power fields (10x) were randomly selected. The percentage of area occupied by positive cells was calculated for each field.

Finally, immunohistochemistry was performed using antibodies against MAC387 (1:500, DAKO) and CD163 (Neat, INIA, Spain) incubated overnight at 4°C. Subsequently, both antibodies were incubated with EnVision®+ System-HRP (DAKO) for 45 min at room temperature and revealed with diaminobenzidine-hydrogen peroxide

346 solution for 10 min. Finally, slides were additionally stained using Prussian blue as
347 described above.
348
349 **2.11 ELISPOT assay**
350 One or two weeks after immunisation, PBMCs and InLN cells were collected and
351 analyzed for specific IFN-γ production by ELISPOT following manufacturer's
352 instructions (Becton Dickinson, UK). Briefly, PBMCs were isolated by Histopaque-
353 1.077® gradient and plated in duplicate at 5 x 10^5/100 µL/well in RPMI-1640
354 supplemented with 10% foetal calf serum (FCS) into 96-well plates (MultiScreen®
355 MAHAS4510 Millipore). InLN cells were isolated in PBS using scalpel and scissors,
356 passed through 70 and 45 µm filters and plated in duplicate at 10^4 and 10^3/100 µL/well.
357 Plates were coated overnight at 4ºC with 5 µg/mL anti-pig IFN-γ-specific capture mAb
358 (P2G10, Becton Dickinson UK) 100 µL/well. For the *in vitro* antigen recall, 35 µg/mL
359 of 3A peptide or 20 µg/mL of RHDV-VLPs and RHDV-3A-VLPs were used as stimuli.
360 As positive control, cells were incubated with 10 µg/mL phytohaemagglutinin (PHA)
361 (Sigma) and cells incubated in the absence of antigen were used as negative control.
362 Plates were cultured for 72 h at 37ºC, then incubated with 2 µg/mL of biotinylated anti-
363 IFN-γ mAb (P2C11, Becton Dickinson), followed by streptavidin-horseradish
364 peroxidase conjugates (Jackson Immunoresearch Lab.). The presence of IFN-γ-
365 producing cells was visualised using 3-Amino-9-Ethylcarbazole (AEC) substrate
366 (Sigma). The background values (number of spots in negative control wells) were
367 subtracted from the respective counts of the stimulated cells and immune responses
368 were expressed as number of spots per million of PBMCs or InLN cells. Data are
369 representative of two different assays performed with the samples.
370

2.13 Statistical analysis

All statistical analysis was performed using SPSS 15.0 software (SPSS Inc., Chicago, IL, USA). For all analyses, each pig was used as the experimental unit. The significance level (α) was set at 0.05 with statistical tendencies reported when $P<0.10$. A non-parametric test (Kruskal-Wallis) was chosen to compare the different values obtained for the immunological parameters and histopathological scores between groups in the different experiments. This non-parametric analysis was chosen due to the number of animals used in each experimental group. Finally, a Fisher exact test was used to test the association between histopathological observations (presence or absence of secondary lymphoid follicles) and the experimental group.

3. Results

3.1 Phenotype and functional characterization of SPIO-labelled MoDCs

To assess the question of whether SPIO labelling procedure and the engulfed iron may cause any changes in the viability and immunological properties of the poMoDCs, different functional assays were performed *in vitro*. Firstly, titration experiments were performed to test the effect of SPIO particles in mature MoDC culture. Labelling of poMoDCs with SPIO altered in some way poMoDCs viability; in fact, mortality around 30% was observed by trypan blue and by flow cytometry when poMoDCs were incubated with 12-50 µg Fe/mL (**Fig. 1A**). Similar values were obtained when human MoDCs were incubated with 200 µg Fe/mL SPIO (**Fig. 1B**), meaning that around 70% of the porcine SPIO-MoDCs were viable in the culture.

On the other hand, labelling efficiency using 25 µg Fe/mL was around 95%, as shown by Perls staining of SPIO-poMoDC culture (Supplementary data **Fig. 8, 4**). Thus, a

range between 25 and 50 µg Fe/mL of SPIO concentration was considered appropriate for *in vitro* and *in vivo* studies. At day 6, SPIO-poMoDCs morphology was consistent with previous studies in other porcine (Peng et al., 2013) or murine (Baumjohann et al., 2006) cells, with clustered brownish particles in the cell cytoplasm (Supplementary data **Fig. 8A, 2-3**). The phenotype of poMoDCs was consistent with previous studies (Carrasco et al., 2001; Crisci et al., 2012b) and the phenotype of SPIO-labelled and unlabelled poMoDCs appeared quite similar and consistent with mature poMoDCs, except for the expected SPIO labelled-cell complexity enhancement showed by the SSC (**Fig. 2A**). Flow cytometry analysis of all markers revealed no statistically significant changes in the surface expression of molecules involved in antigen capture (CD163), presentation (MHC class II, I) and co-stimulation (CD80/86) between mock/unlabelled MoDCs and SPIO-MoDCs. Only a slightly decrease in surface markers intensity was visible in SPIO culture comparing with mock DCs (**Fig. 2A**). Phenotype of SPIO-MoDCs was similar to mock MoDCs after LPS stimulation and up-regulation of SLAII (data not shown) and CD80/86 (**Fig. 2A**) was observed in both cultures.

Similar results were obtained testing SPIO in huMoDCs (Supplementary data **Fig. 8**). SPIO labelled huMoDCs showed brownish cytoplasmatic particles (Supplementary data **Fig. 8A**) and maintained the expression of cell surface markers as mock culture (**Fig. 3A**). This phenotype was consistent with mature huMoDCs. SPIO concentration of 200 µg Fe/mL used for huMoDCs was previously established in (de Vries et al., 2005) to be optimal in terms of viability and cell labelling. Nevertheless, additional viability testing was performed in huMoDCs using SPIO at 200 µg Fe/mL and the results showed that cell viability was around 70% (**Fig. 1B**).

Cytokine production was determined in supernatants of both mock and SPIO-poMoDCs cultured in the presence or absence of RHDV-3A-VLPs or LPS at 24 h. TNF-α

production was similar ($p>0.05$) between SPIO-labelled and unlabelled poMoDCs (**Fig. 2B**) in the range of 25-50 μg Fe/mL of SPIO. The same pattern was obtained with IL-6 (data not shown). Finally, using MLR test, the functionality of poSPIO-MoDCs compared with mock cells was evaluated. Both poMoDC cultures induced similar PBLs proliferation pattern when incubated alone or with RHDV-3A-VLP for 4 days (**Fig. 2C**).

Likewise, human SPIO labelled MoDCs maintained their functionality as revealed by MLR assay measuring proliferation (**Fig. 3B**) and IFN-γ production (**Fig. 3C**). Statistically significant differences between groups ($p>0.05$) were not observed. Together these results demonstrated that SPIO labelling did not affect DC functionality, being a suitable candidate for *in vivo* cell tracking.

3.2 *In vivo* MRI tracking

Because the functional assays described above did not show strong reductions in the immunological key features of MoDCs by labelling procedures, poSPIO-MoDCs were used for *in vivo* MRI detection after their SC inoculation. Small hypointense signals or signal voids could be observed in the right inguinal subcutaneous tissue at all three time points post inoculation. Similarly, multifocal signal voids up to 3.8 mm in diameter were present in the right and left inguinal lymph nodes. The signal voids were already present in the right lymph node at 20 min, and they were visible in both lymph nodes, although being always larger in the right one at 30 h and 46 h (**Fig. 4**, arrows).

3.3 Histology and immunohistochemistry of regional lymph nodes

In pigs, lymphoid follicles are located in the center of the lymph node, rather than in the periphery as in the rest of domestic animals (**Fig. 5A**). These can be observed in **figure**

446 **5B**, where few secondary follicles are indicated by arrows. In **figure 5C**, higher
447 numbers of secondary follicles are observed. Histopathological analysis of the
448 superficial InLNs revealed some grade or reactivity in the lymph nodes in all the
449 experimental groups (in a range of 33 to 66% of the animals) with the exception of the
450 control group (0%). No statistically significant differences were observed between
451 experimental groups, probably due to low statistical potency of the experimental design
452 (2 or 3 animals by group) (**Table 2**).
453 Additionally, localization of SPIO-labelled DCs in the InLNs was further confirmed by
454 histology after Prussian blue staining of sections (**Fig. 5**). Piglets inoculated with SPIO
455 labelled DCs showed iron-containing cells in the paracortex and subcapsular area of
456 both InLNs (**Fig. 5 D, E**). Moreover, piglets inoculated with RHDV-3A-VLP pulsed
457 SPIO-MoDCs showed higher level of Prussian blue positive cells (**Fig. 5D** left InLN
458 and **5E** right InLN). Higher positivity correlated to higher SPIO concentration used for
459 labelled DC generation (**Table 2**). Similar pattern was observed in the InLNs from pig
460 monitored by MRI (data not shown).
461 One question was whether or not SPIO-containing cells in the lymph nodes were
462 macrophages that had phagocytosed SPIO-poMoDC or cell-free SPIO particles released
463 from dead cells. The results in **figure 5** showed that the majority of SPIO-containing
464 cells were negative for *bona fide* macrophage markers as MAC387 (Chianini et al.,
465 2001) and CD163 (Bullido et al., 1997) (**Fig. 5, F** and **G** respectively), indicating that
466 SPIO-positive cells were not macrophages and suggesting that they were SPIO-MoDCs.
467

468 **3.4 DC immunization stimulate specific systemic and local responses**

469 To get insight into the possibility to use pigs as model for DC-based immunization test,
470 local and systemic cell-mediated responses induced by RHDV-3A-VLP and RHDV-

VLP-pulsed MoDCs immunization were studied. PBMCs or InLN cells were tested one or two weeks after immunization for studying systemic and local responses respectively. In the case of systemic responses, two weeks after the DC immunization of animals with RHDV-3A-VLP, specific IFN-γ-secreting cells against peptide 3A were detected in PBMCs from RHDV-3A-VLP pulsed MoDC group by ELISPOT (**Fig. 6**). As expected, animals in the RHDV-VLP pulsed MoDC group did not show any specific 3A response (**Fig. 6**). Unsurprisingly, animals treated with RHDV-3A-VLP or with RHDV-VLP pulsed MoDC showed IFN-γ-secreting cells against RHDV-VLP and RHDV-3A-VLP (**Fig. 6**). Animals treated with RHDV-VLP pulsed MoDC showed higher response compared to animals treated with RHDV-3A-VLP pulsed MoDC after RHDV-VLP stimulation (**Fig. 6**).

Analysis of local responses in InLN revealed that animals treated with RHDV-3A-VLP or with RHDV-VLP pulsed MoDC were able to induce higher number of specific IFN-γ-secreting InLN cells against RHDV-VLP and RHDV-3A-VLP comparing to unpulsed animals (**Fig. 6**). An interesting finding was that RHDV-3A-VLP pulsed SPIO-MoDC immunization was also able to induce specific systemic and local responses against all the antigens used in the ELISPOT assay (**Fig. 6**). No statistically significant differences were observed between experimental groups, probably due to low statistical potency of the experimental design (2 or 3 animals by group). As expected, in all the assays, control pigs and unpulsed-MoDC-immunized pigs did not show any significant response or background level.

4. Discussion

In vivo serial tracking of porcine SPIO mesenchymal stem cells (MSCs) can be achieved by MRI and miniature Tibetan swine, which have shown to be ideal animals

for researching heart function (Yang et al., 2011). However, no studies so far have addressed tracking SPIO-loaded DC in pigs. To the best of our knowledge, this is the first report of tracking of SPIO-labelled DCs in pigs by non-invasive MRI technology, which was confirmed by histology. Interestingly, antigen-loaded SPIO-DCs were located with the draining lymph nodes and they were able to induce specific immune responses after cell administration.

In our study, porcine MoDCs were labelled in the immature state, when they are highly phagocytic (Banchereau and Steinman, 1998), increasing the probability of intracellular magnetic labelling with SPIO particles. The most effective iron concentration for labelling porcine DCs led to an optimal ratio of 25-50 µg Fe/mL in our system. The phenotype and functional properties of the SPIO-labelled DCs were slightly altered as compared with unlabelled DCs. Our work was in line with a previous study performed in mice (de Chickera et al., 2011). Nevertheless, any changes in other parameters tested such as cytokine production and T cell activation (as T cell proliferation) could not be observed, confirming *in vitro* the functionality of SPIO-MoDCs. Thus, having shown that pig-derived DCs can be labelled with SPIO without affecting its functional properties, further studies were conducted to follow the migration of autologous *ex vivo*-cultured SPIO-MoDCs after subcutaneous administration into the inguinal zone of pigs. SPIO-MoDCs were tracked *in vivo* by MRI to determine their migratory behaviour after subcutaneous injection.

The major advantage of MRI is a superior anatomical correlation and spatial resolution, which allows precise localization of SPIO-labelled DCs at the actual injection site and after migration. Although *in vivo* imaging provided us with a lot of information on the distribution of the DC immunization after injection, technical restrictions limited the

results in porcine lymph nodes to be positive/negative for cell-tracking label, as it was also previously described in human by Verdijk et al. (Verdijk et al., 2009). In fact, the low resolution of the MR used in this study was not sufficient for monitoring the precise localization of SPIO-DCs. These results paved the way for future studies with higher MRI resolution to analyse DC interaction within lymph nodes in more detail.

Specific signal in the lymph node was detected after subcutaneous injection of around half a million of SPIO-MoDCs. Thus, this technological approach was able to detect a relative low amount of labelled-DCs in the InLN, which we were not able to quantify. However, previous studies have shown that after intradermal injection hardly 4% of DCs migrated to the draining lymph nodes (Verdijk et al., 2009) and after subcutaneous injection only the 1-2% (Baumjohann et al., 2006; MartIn-Fontecha et al., 2003). If this percentage were to be applied in our experimental conditions in swine, MRI would be able to detect around 5,000-10,000 labelled cells in superficial InLNs. The pattern of the labelling from those studies compared to the one presented here was rather similar, as shown in (**Fig. 4, 5**, (Baumjohann et al., 2006)) and probably it was due to the fact that InLNs are very superficial and the migration from the site of inoculation was very rapid, as confirmed by the MRI performed 20 min after administration. Furthermore, higher signal from SPIO pulsed DC was detected in the right InLN (closest to the inoculation site) but signal voids were also present in the left one.

The fact that pig can be used as model for testing DC tracking *in vivo* is particularly relevant. Further optimization for cell-based therapies in human is required but the data presented here the proof of concept. In fact, domestic pigs represent an excellent animal model for immunological studies, since they are outbred animals that better resemble the variability of human population and experiments in pigs are much more likely to be predictive of therapeutic treatments in humans than experiments in rodents. *In vivo*

following of therapeutic cells primarily tracks the cell label and may need to be confirmed with immunohistochemical studies. Depending on the method of administration and the nature of the vaccine, immunohistochemical analysis of target organs will still be decisive for quantitative and qualitative evaluation of the efficacy of cellular therapy (Verdijk et al., 2009).

Subsequently, histological analysis and Prussian blue staining of porcine tissue sections from dissected lymph nodes was used to visualize SPIO-labelled cells offering further validation to track mixed cell populations at single-cell level, something that cannot be possible in the case of human trials. The data in this study revealed that paracortex and subcapsular areas of the lymph node were positive for Prussian blue staining and the presence of SPIO-labelled DCs correlated with the concentration of iron particles used during DC generation. This location resembled the one reported in previous DC migration studies performed in human (de Vries et al., 2005) and mice (Baumjohann et al., 2006). Additionally, the pattern of immunohistochemistry staining have shown that the majority of the $Perls^{+}$ cells were not from *bona fide* macrophage markers, suggesting that they might indeed correspond to injected pulsed DCs and the signal was mainly not due to macrophages that had phagocytosed cell-free SPIO particles released from dead cells or SPIO pulsed DC. However, a small percentage of phagocytosis of free SPIO particles or dead $SPIO^{+}$ cells by APC cannot be excluded to occur in this system.

Once it was shown that pulsed DC were functional *in vitro* and they were able to migrate from the site of injection to the regional lymph nodes, the question to answer was whether these pulsed DC were able to elicit a specific immune response. Production of specific IFN-γ producing cells against the vector (RHDV-VLPs) and also against the antigenic epitope inserted into the VLPs (3A) after one or two weeks post inoculation was shown (**Fig. 6**). These results indicated that these pulsed DC were

functionally active *in vivo*. Despite of the lack of statistical significance of the data, pigs were able to induce not only specific local and but also systemic responses.

In this study, subcutaneous inoculation was used since it is one of the most frequently route used to treat solid tumors in human (Verdijk et al., 2009) and also because it allowed us to track the cells in accessible lymph nodes in pigs. Nevertheless, other routes or combination of them may be tested in further studies using higher resolution MRI.

In conclusion, this is the first study demonstrating the potential of using MRI for tracking DCs in pigs and showed how these animals represent an excellent and closer animal models to human than rodents to monitor and optimize DC-based therapies. The results in this proof-of-principle study pave the way to use pig as model for a variety of DC studies *in vivo*, which might be of pivotal importance for cell immunotherapy in humans in the future.

5. Acknowledgements

We want to thank: Ferrán López, Rosa López, Zoraida Cervera, Pamela Martinez-Orellana, Tufaria Mussá, Massimiliano Baratelli, Diego Pérez, Sergio López from CRESA and José Luis Ruiz de la Torre and Javier Aceña (UAB) for farm and technical support; Jaume Martorell (Fundació Hospital Clínic Veterinari, UAB) for MRI support; Javier Domínguez (INIA) for the porcine antibodies; Antonio Lestuzzi, Michele Crisci and Raif Yucel for MR imaging support; Joaquim Segalés for anatomic pathology analysis; Mónica Pérez for immunohistochemical stainings; Aida Neira and Blanca Pérez for Perls staining; Eva Huerta y Marina Sibila for PCV2 PCR; David Andreu and

Beatriz García de la Torre (Pompeu Fabra University, Barcelona), and Esther Blanco (CISA-INIA, Madrid), for the FMDV 3A peptide; Alicia Solórzano for critically reviewing the manuscript. This work was funded by the project AGL2010-22200-C02 of Spanish Ministry of Science and Innovation. PhD studies of Raquel Cabezón are funded by a doctoral FI fellowship from the Generalitat de Catalunya.

6. Conclusions

- Human or pig dendritic cells pulsed with superparamagnetic iron oxide particles did not alter their phenotypic and functional properties *in vitro* in the experimental conditions tested in this work.
- After subcutaneous inoculation in pigs, porcine SPIO-MoDC migration to regional lymph nodes was detected by MRI and confirmed by Perls staining of draining lymph nodes.
- Only one dose of virus-like particles-pulsed MoDCs in pigs was able to induce specific local and systemic responses.
- This proof-of-principle study shows the potential of using pigs as a suitable animal model to test DC trafficking with the aim of improving cellular therapies.

7. References

Aarntzen E. H., de Vries I. J., Goertz J. H., Beldhuis-Valkis M., Brouwers H. M., van de Rakt M. W., van der Molen R. G., Punt C. J., Adema G. J., Tacken P. J., Joosten I. and Jacobs J. F. (2012) Humoral anti-KLH responses in cancer

patients treated with dendritic cell-based immunotherapy are dictated by different vaccination parameters. *Cancer Immunol Immunother* **61**, 2003-11.

Ardon H., Van Gool S. W., Verschuere T., Maes W., Fieuws S., Sciot R., Wilms G., Demaerel P., Goffin J., Van Calenbergh F., Menten J., Clement P., Debiec-Rychter M. and De Vleeschouwer S. (2012) Integration of autologous dendritic cell-based immunotherapy in the standard of care treatment for patients with newly diagnosed glioblastoma: results of the HGG-2006 phase I/II trial. *Cancer Immunol Immunother* **61**, 2033-44.

Banchereau J. and Palucka A. K. (2005) Dendritic cells as therapeutic vaccines against cancer. *Nat Rev Immunol* **5**, 296-306.

Banchereau J. and Steinman R. M. (1998) Dendritic cells and the control of immunity. *Nature* **392**, 245-52.

Barcena J., Verdaguer N., Roca R., Morales M., Angulo I., Risco C., Carrascosa J. L., Torres J. M. and Caston J. R. (2004) The coat protein of Rabbit hemorrhagic disease virus contains a molecular switch at the N-terminal region facing the inner surface of the capsid. *Virology* **322**, 118-34.

Baumjohann D., Hess A., Budinsky L., Brune K., Schuler G. and Lutz M. B. (2006) In vivo magnetic resonance imaging of dendritic cell migration into the draining lymph nodes of mice. *Eur J Immunol* **36**, 2544-55.

Baumjohann D. and Lutz M. B. (2006) Non-invasive imaging of dendritic cell migration in vivo. *Immunobiology* **211**, 587-97.

Bullido R., Gomez del Moral M., Alonso F., Ezquerra A., Zapata A., Sanchez C., Ortuno E., Alvarez B. and Dominguez J. (1997) Monoclonal antibodies specific for porcine monocytes/macrophages: macrophage heterogeneity in the pig evidenced by the expression of surface antigens. *Tissue Antigens* **49**, 403-13.

646 Bulte J. W. and Kraitchman D. L. (2004) Monitoring cell therapy using iron oxide MR
647 contrast agents. *Curr Pharm Biotechnol* **5**, 567-84.
648 Carrasco C. P., Rigden R. C., Schaffner R., Gerber H., Neuhaus V., Inumaru S.,
649 Takamatsu H., Bertoni G., McCullough K. C. and Summerfield A. (2001)
650 Porcine dendritic cells generated in vitro: morphological, phenotypic and
651 functional properties. *Immunology* **104**, 175-84.
652 Chianini F., Majo N., Segales J., Dominguez J. and Domingo M. (2001)
653 Immunohistological study of the immune system cells in paraffin-embedded
654 tissues of conventional pigs. *Vet Immunol Immunopathol* **82**, 245-55.
655 Crisci E., Almanza H., Mena I., Cordoba L., Gomez-Casado E., Caston J. R., Fraile L.,
656 Barcena J. and Montoya M. (2009) Chimeric calicivirus-like particles elicit
657 protective anti-viral cytotoxic responses without adjuvant. *Virology* **387**, 303-12.
658 Crisci E., Barcena J. and Montoya M. (2012a) Virus-like particles: The new frontier of
659 vaccines for animal viral infections. *Vet Immunol Immunopathol* **148**, 211-25.
660 Crisci E., Fraile L., Moreno N., Blanco E., Cabezon R., Costa C., Mussa T., Baratelli
661 M., Martinez-Orellana P., Ganges L., Martinez J., Barcena J. and Montoya M.
662 (2012b) Chimeric calicivirus-like particles elicit specific immune responses in
663 pigs. *Vaccine* **30**, 2427-39.
664 Cubillos C., Garcia de la Torre B., Barcena J., Andreu D., Sobrino F. and Blanco E.
665 (2012) Inclusion of a specific T cell epitope increases the protection conferred
666 against foot-and-mouth disease virus in pigs by a linear peptide containing an
667 immunodominant B cell site. *Virol J* **9**, 66.
668 de Chickera S. N., Snir J., Willert C., Rohani R., Foley R., Foster P. J. and Dekaban G.
669 A. (2011) Labelling dendritic cells with SPIO has implications for their

subsequent in vivo migration as assessed with cellular MRI. *Contrast Media Mol Imaging* **6**, 314-27.

de Vries I. J., Lesterhuis W. J., Barentsz J. O., Verdijk P., van Krieken J. H., Boerman O. C., Oyen W. J., Bonenkamp J. J., Boezeman J. B., Adema G. J., Bulte J. W., Scheenen T. W., Punt C. J., Heerschap A. and Figdor C. G. (2005) Magnetic resonance tracking of dendritic cells in melanoma patients for monitoring of cellular therapy. *Nat Biotechnol* **23**, 1407-13.

Ezquerra A., Revilla C., Alvarez B., Perez C., Alonso F. and Dominguez J. (2009) Porcine myelomonocytic markers and cell populations. *Dev Comp Immunol* **33**, 284-98.

Figdor C. G., de Vries I. J., Lesterhuis W. J. and Melief C. J. (2004) Dendritic cell immunotherapy: mapping the way. *Nat Med* **10**, 475-80.

Giannoukakis N., Phillips B., Finegold D., Harnaha J. and Trucco M. (2011) Phase I (safety) study of autologous tolerogenic dendritic cells in type 1 diabetic patients. *Diabetes Care* **34**, 2026-32.

Hilkens C. M. and Isaacs J. D. (2013) Tolerogenic dendritic cell therapy for rheumatoid arthritis: where are we now? *Clin Exp Immunol* **172**, 148-57.

Hoehn M., Wiedermann D., Justicia C., Ramos-Cabrer P., Kruttwig K., Farr T. and Himmelreich U. (2007) Cell tracking using magnetic resonance imaging. *J Physiol* **584**, 25-30.

Long C. M., van Laarhoven H. W., Bulte J. W. and Levitsky H. I. (2009) Magnetovaccination as a novel method to assess and quantify dendritic cell tumor antigen capture and delivery to lymph nodes. *Cancer Res* **69**, 3180-7.

Luque D., Gonzalez J. M., Gomez-Blanco J., Marabini R., Chichon J., Mena I., Angulo I., Carrascosa J. L., Verdaguer N., Trus B. L., Barcena J. and Caston J. R. (2012)

695 Epitope insertion at the N-terminal molecular switch of the rabbit hemorrhagic
696 disease virus T = 3 capsid protein leads to larger T = 4 capsids. *J Virol* **86**, 6470-
697 80.
698 MartIn-Fontecha A., Sebastiani S., Hopken U. E., Uguccioni M., Lipp M.,
699 Lanzavecchia A. and Sallusto F. (2003) Regulation of dendritic cell migration to
700 the draining lymph node: impact on T lymphocyte traffic and priming. *J Exp*
701 *Med* **198**, 615-21.
702 Metz S., Bonaterra G., Rudelius M., Settles M., Rummeny E. J. and Daldrup-Link H. E.
703 (2004) Capacity of human monocytes to phagocytose approved iron oxide MR
704 contrast agents in vitro. *Eur Radiol* **14**, 1851-8.
705 Meurens F., Summerfield A., Nauwynck H., Saif L. and Gerdts V. (2012) The pig: a
706 model for human infectious diseases. *Trends Microbiol* **20**, 50-7.
707 Nestle F. O., Farkas A. and Conrad C. (2005) Dendritic-cell-based therapeutic
708 vaccination against cancer. *Curr Opin Immunol* **17**, 163-9.
709 Peng C., Yang K., Xiang P., Zhang C., Zou L., Wu X., Gao Y., Kang Z., He K., Liu J.,
710 Cheng M., Wang J. and Chen L. (2013) Effect of transplantation with
711 autologous bone marrow stem cells on acute myocardial infarction. *Int J Cardiol*
712 **162**, 158-65.
713 Randolph G. J., Angeli V. and Swartz M. A. (2005) Dendritic-cell trafficking to lymph
714 nodes through lymphatic vessels. *Nat Rev Immunol* **5**, 617-28.
715 Raynal I., Prigent P., Peyramaure S., Najid A., Rebuzzi C. and Corot C. (2004)
716 Macrophage endocytosis of superparamagnetic iron oxide nanoparticles:
717 mechanisms and comparison of ferumoxides and ferumoxtran-10. *Invest Radiol*
718 **39**, 56-63.

719 Rogers W. J., Meyer C. H. and Kramer C. M. (2006) Technology insight: in vivo cell
720 tracking by use of MRI. *Nat Clin Pract Cardiovasc Med* **3**, 554-62.
721 Schuler G., Schuler-Thurner B. and Steinman R. M. (2003) The use of dendritic cells in
722 cancer immunotherapy. *Curr Opin Immunol* **15**, 138-47.
723 Silva-Campa E., Cordoba L., Fraile L., Flores-Mendoza L., Montoya M. and Hernandez
724 J. (2010) European genotype of porcine reproductive and respiratory syndrome
725 (PRRSV) infects monocyte-derived dendritic cells but does not induce Treg
726 cells. *Virology* **396**, 264-71.
727 Summerfield A. and McCullough K. C. (2009) The porcine dendritic cell family. *Dev*
728 *Comp Immunol* **33**, 299-309.
729 Verdijk P., Aarntzen E. H., Lesterhuis W. J., Boullart A. C., Kok E., van Rossum M.
730 M., Strijk S., Eijckeler F., Bonenkamp J. J., Jacobs J. F., Blokx W., Vankrieken
731 J. H., Joosten I., Boerman O. C., Oyen W. J., Adema G., Punt C. J., Figdor C. G.
732 and de Vries I. J. (2009) Limited amounts of dendritic cells migrate into the T-
733 cell area of lymph nodes but have high immune activating potential in
734 melanoma patients. *Clin Cancer Res* **15**, 2531-40.
735 Wilgenhof S., Van Nuffel A. M., Benteyn D., Corthals J., Aerts C., Heirman C., Van
736 Riet I., Bonehill A., Thielemans K. and Neyns B. (2013) A phase IB study on
737 intravenous synthetic mRNA electroporated dendritic cell immunotherapy in
738 pretreated advanced melanoma patients. *Ann Oncol* **24**, 2686-93.
739 Yang K., Xiang P., Zhang C., Zou L., Wu X., Gao Y., Kang Z., He K., Liu J. and Peng
740 C. (2011) Magnetic resonance evaluation of transplanted mesenchymal stem
741 cells after myocardial infarction in swine. *Can J Cardiol* **27**, 818-25.
742
743

8. Figure legends

Fig. 1.Viability test of SPIO labeled porcine and human MoDCs.

Viability of SPIO-MoDCs was assessed by flow cytometry using LIFE/DEAD Fixable Dead Cell Stain Kit and FITC-conjugated Annexin V. (**A**) PoMoDCs were incubated with 50 µg Fe/mL of SPIO particles. This is a representative experiment from two independent experiments performed using poMoDCs from two different animals. Gate strategy is showed in a representative plot. (**B**) HuMoDCs were incubated with SPIO at 200 µg Fe/mL. This is a mean+SD from two independent experiments performed using HuMoDCs generated from two different donors. Gate strategy is showed in a representative plot.

Fig. 2. Morphology and phenotype of SPIO-labelled porcine dendritic cells.

A) Phenotype of porcine SPIO-MoDCs compared with mock culture at day 6. Similar patterns for CD172a, SLAII, CD163 and CD80/86 molecules were observed when MoDCs were incubated with a range of 25-50 µg Fe/mL of SPIO particles. Light grey histogram shows the isotype control. After LPS stimulation, the up-regulation of CD80/86 marker (black line) was consistent in SPIO-MoDCs and mock culture. Dark grey histograms with dotted line show the marker expression in un-stimulated DCs and light grey the isotype control. **B)** Cytokine production after LPS and RHDV-3A-VLP stimulation. TNF-α production in SPIO-MoDCs (30 µg Fe/mL) (black histograms) and mock culture (white histograms) at 24 h. **C)** Mixed lymphocyte reaction. Effect on PBLs activation by pulsed MoDCs. Untreated MoDCs (white) and SPIO-MoDC (black) were co-cultured with allogeneic PBLs (ratio 1:20, respectively). Four days after, co-culture proliferation was evaluated using CFSE. PBLs co-cultured with mock MoDCs

769 or SPIO-MoDCs were used as negative control. Data represents the mean ± SD (n = 4)
770 and are representative of three independent experiments with different animals.
771
772 **Fig. 3. Morphology, phenotype and immunogenicity of SPIO-labelled human**
773 **dendritic cells.**
774 **A)** Phenotype of human SPIO-MoDCs compared with mock culture at day 7. Similar
775 expression patterns for CD80, CD83, CD86 and HLA-DR molecules were observed
776 when huMoDCs were incubated with 200 µg/mL of SPIO particles. Grey histogram
777 shows the isotype control. **B)** Mixed lymphocyte reaction. Untreated HuMoDCs (black)
778 and SPIO-huMoDC (grey) were co-cultured with allogeneic PBLs (ratio 1:20,
779 respectively). Six days after, co-culture proliferation was evaluated using tritiated
780 thymidine. **C)** IFN-γ production by T cells was tested in the supernatant of MLR using
781 ELISA. Data represents the mean ± SD of triplicates and are representative of four
782 independent experiments with different donors (n = 4).
783
784 **Fig. 4. MRI of superficial inguinal lymph nodes and site of inoculation.**
785 SPIO-MoDCs inoculated pig from group E using 50 µg Fe/ml. T2* Transverse MRI
786 slices at the level of the InLNs and the site of inoculation before the inoculation (**A**), 20
787 minutes (**B**), 30 h (**C**) and 46 h (**D**) after inoculation. At the site of inoculation, small
788 signal voids are visible in the right subcutaneous tissue (arrow), being more evident 20
789 min after inoculation but still visible 30 h and 46 h after inoculation. **A**) Before
790 inoculation, the InLNs appear as two oval areas (arrows) that show a hyperintense
791 signal compared to the surrounding inguinal fat. Note that the right InLN is larger than
792 the left. **B**) 20 min after inoculation, an oval signal void (arrow) is visible within the
793 lateral aspect of the right InLN. **C**) 30 h after inoculation, multiple small signal voids

(arrows) are also present in the left InLN, which appears more symmetrical with the right than in the previous images. **D**) 46 h after inoculation, an oval signal void (arrow) is still visible within the lateral aspect of the right InLN, whereas no signal voids are visible in the left InLN in this slice. Note: Ventral is to the top, and right is to the left.

Fig. 5. Histopathological analysis of porcine superficial inguinal lymph nodes.

A) Haematoxylin and eosin (H-E), superficial InLN from a control animal (grade -). **B**) H-E, there are small numbers of secondary lymphoid follicles (arrows) (grade +) (group A). Bar = 100 μm. **C)** H-E, moderate numbers of secondary lymphoid follicles (arrows) (grade ++) (group D). Bar = 100 μm. **D**) Perls stain, moderate number of positive cells (grade ++) in subcapsular and paracortical areas (left InLN group F). Bar = 100 μm. **E)** Perls stain, large numbers of positive cells (grade +++) in subcapsular and paracortical areas (right InLN group F). Bar = 100 μm. **F)** Immunohistochemistry, positive cells for MAC387 antibody (brown) are different from those Prussian blue positive cells (blue) (group F). Bar = 100 μm. Inset: particular of MAC^+ cells and SPIO staining with higher magnification, bar = 20 μm. **G)** Immunohistochemistry, the majority of positive cells for CD163 antibody (brown) are different from those Prussian blue positive cells (blue) (group F). Bar = 100 μm. Inset: particular of $Perls^+$ cells and $CD163^+$ cells with higher magnification, bar = 20 μm.

Fig. 6. ELISPOT IFN-γ assay.

Specific local and systemic cellular responses of RHDV-3A-VLP pulsed MoDC and RHDV-3A-VLP pulsed SPIO-MoDC immunised pigs against the vector RHDV-VLP, against the peptide 3A and against chimeric RHDV-3A-VLP at day 7 and 14. Pigs are divided in different groups, depending on the different MoDCs: RHDV-3A-VLP-pulsed

MoDCs (A), RHDV-VLP-pulsed MoDCs (B), control animals (C), unpulsed MoDCs (D) and RHDV-3A-VLP-pulsed SPIO-MoDCs (F). Specific RHDV-VLP, chimeric RHDV-3A-VLP and 3A IFN-γ-producing cells are detected by ELISPOT. The background values (number of spots in negative control wells) were subtracted from the respective counts of the stimulated cells and the immune responses were expressed as number of spots per million of PBMCs or InLN cells for each animal. Shown are the results of duplicate wells for representative data of two repeated experiments.

Fig. 7. Supplementary data. Study design.

Porcine peripheral blood mononuclear cells (PBMCs) were obtained from pigs and monocyte-derived dendritic cells (poMoDCs) where generated by a five-day protocol. PoMoDCs were cultured and labelled with SPIO particles. Then SPIO-DCs were injected subcutaneously into the right inguinal zone and their migration was monitored *in vivo* by MRI of regional lymph nodes. Superficial regional inguinal lymph nodes were obtained after culling and histological studies were performed using Perls staining or immunohistochemistry.

Fig. 8. Supplementary data.

A) Morphology of porcine MoDCs culture with and without SPIO. **A1:** Morphology of poMoDCs at day 6 of culture. Original magnification 200x. **A2**: Morphology of porcine SPIO-MoDCs at day 6 of culture using 25-50 µg Fe/mL of SPIO particles. Original magnification 200x. **A3**: SPIO-poMoDCs in phase contrast image, original magnification 400x. **A4**: Perls staining of SPIO-poMoDC culture with 25 µg Fe/mL of SPIO particles. Bar = 25 µm. **B)** Morphology of human SPIO-MoDCs at day 6 of

843 culture using 200 μg/mL of SPIO particles. Phase contrast image, original magnification
844 200x.
845

Figure 1

Click here to download high resolution image

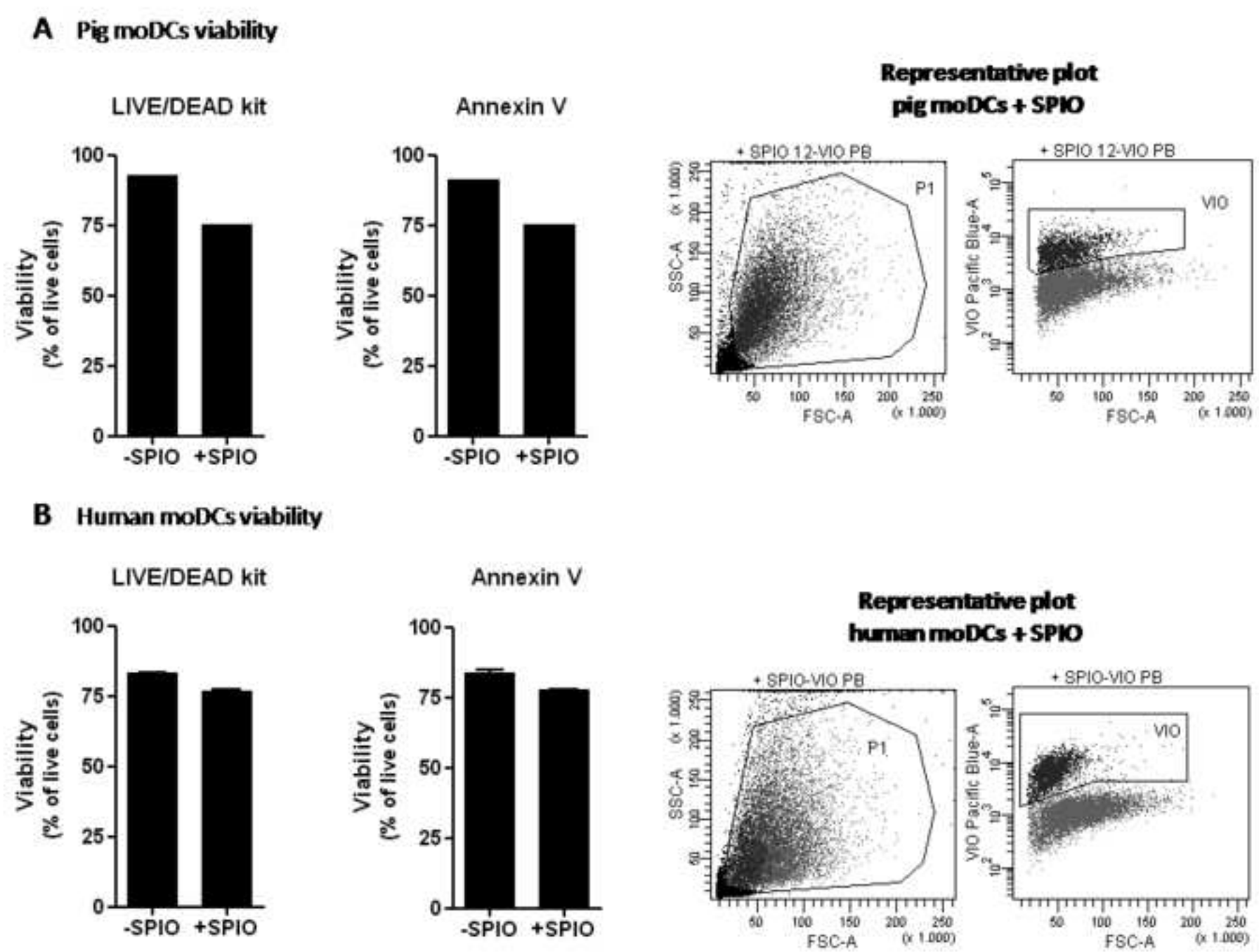

Figure 2

Click here to download high resolution image

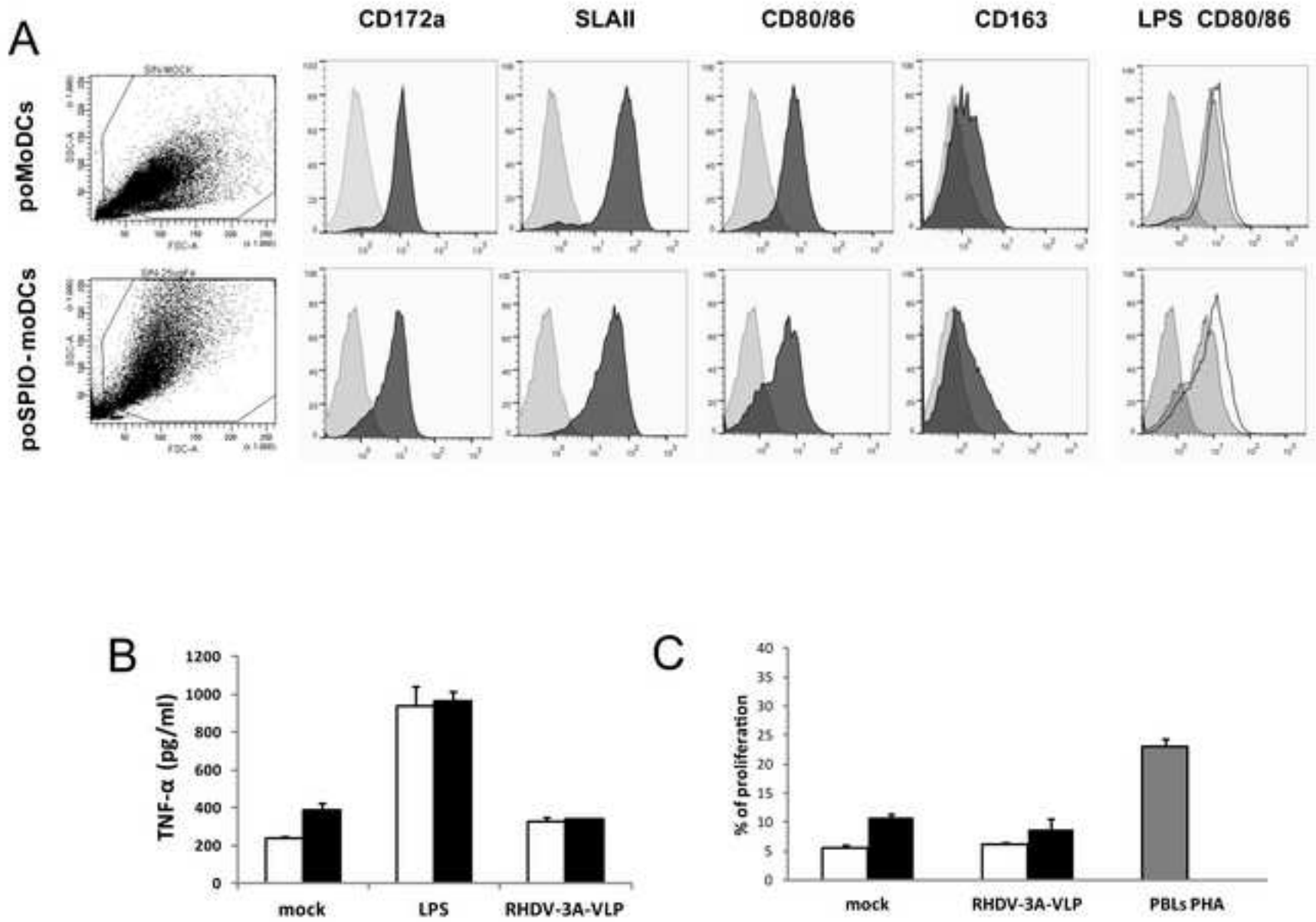

Figure 3

Click here to download high resolution image

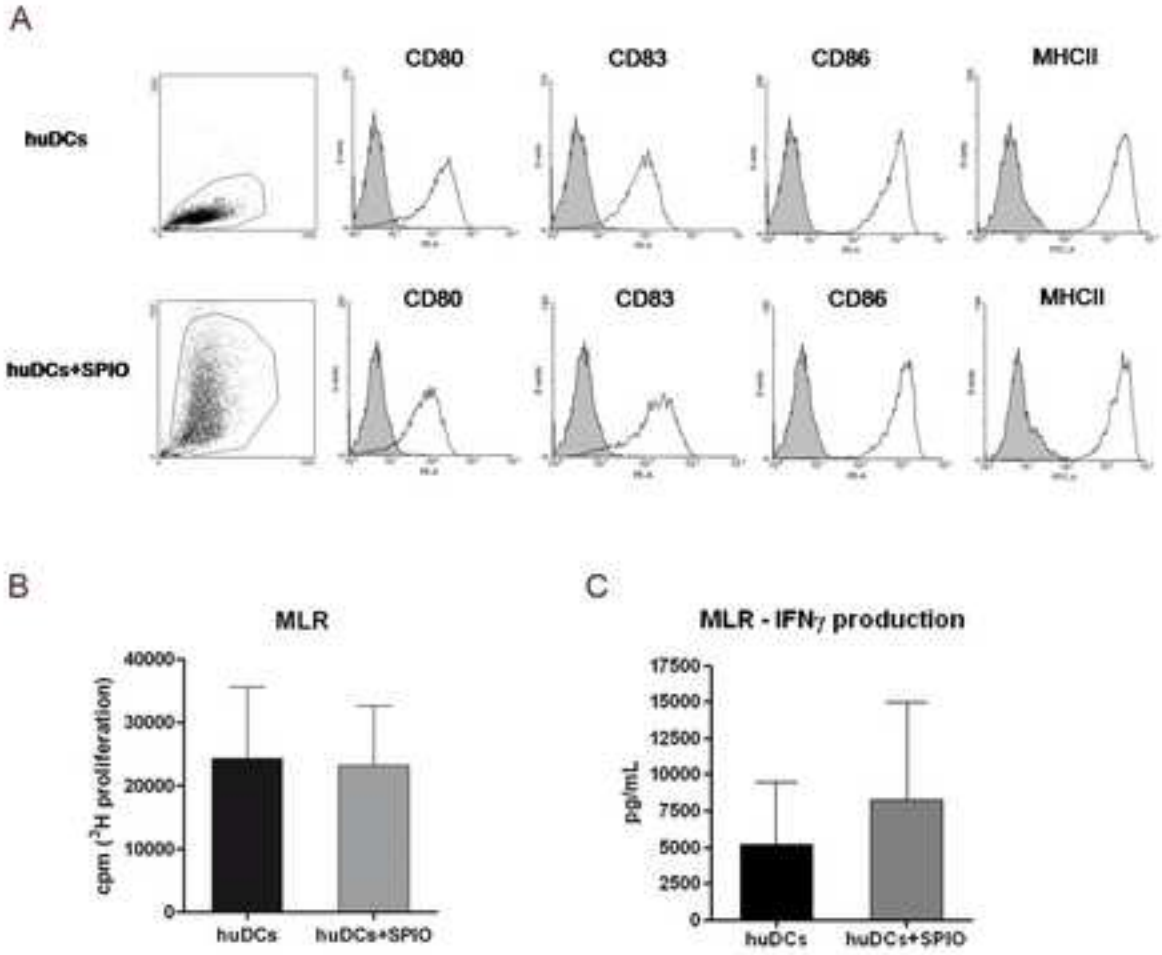

Figure 4

Click here to download high resolution image

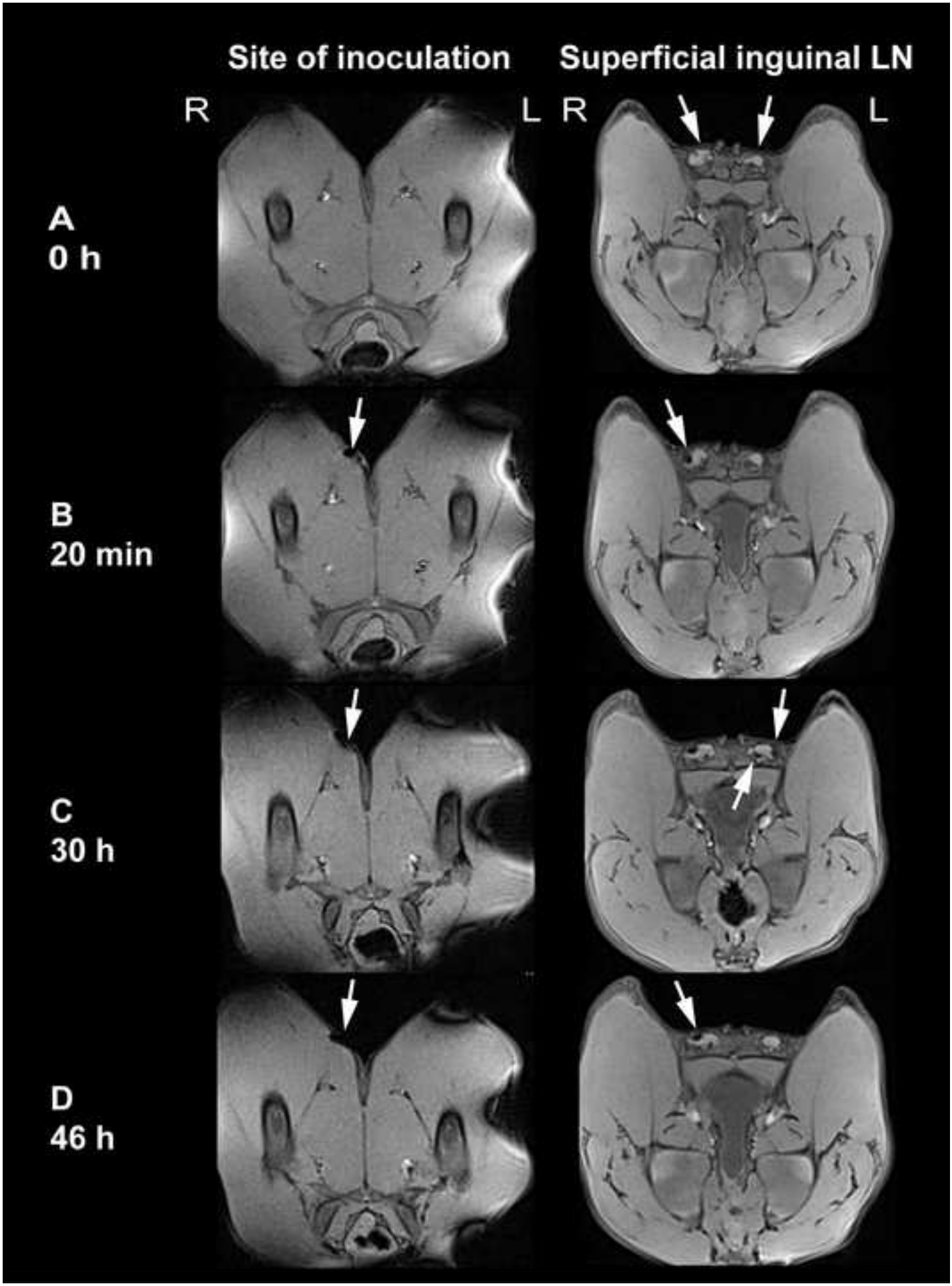

Figure 5

Click here to download high resolution image

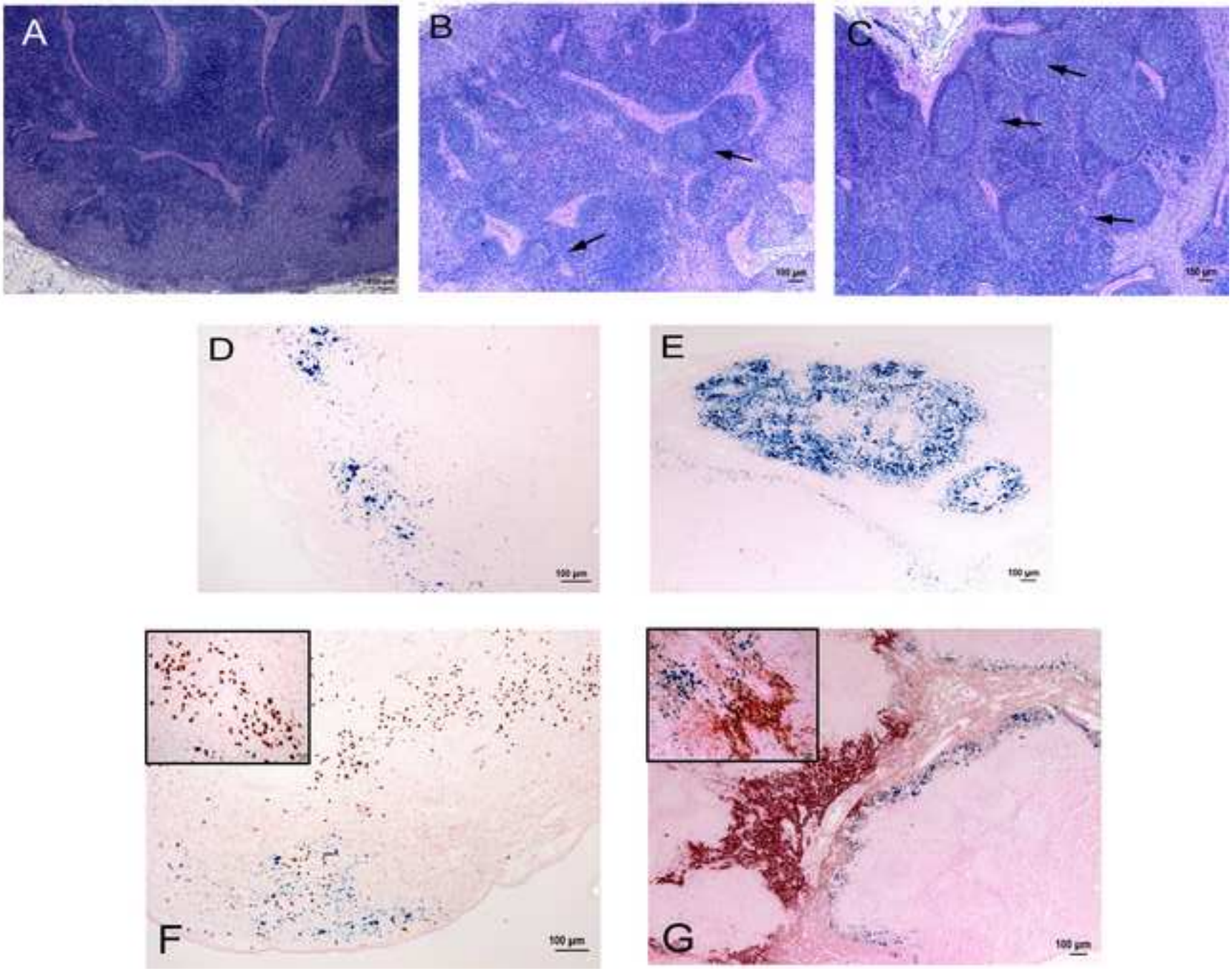

Figure 6

Click here to download high resolution image

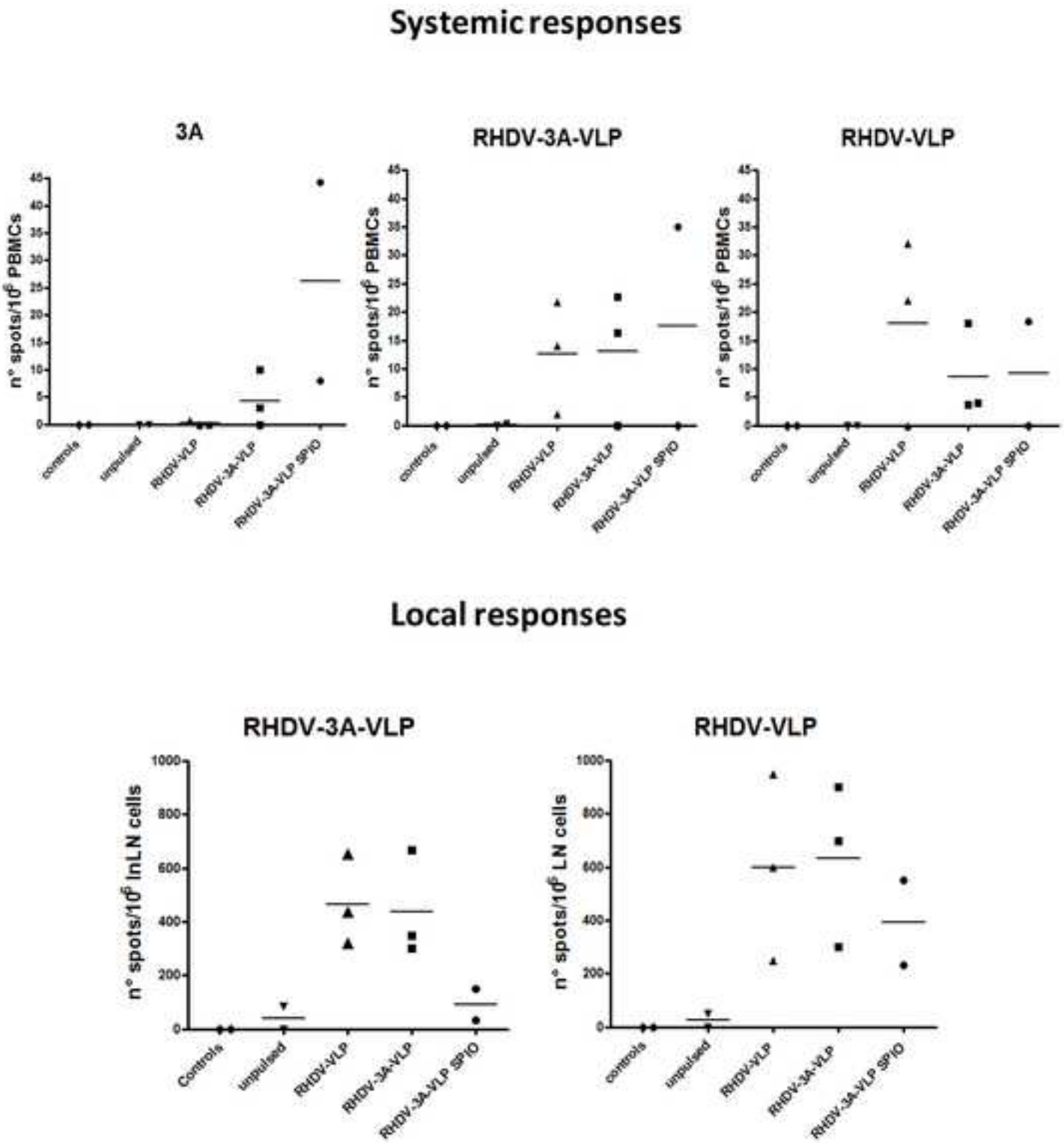

Table 1. *In vivo* experimental designs.

Group	Inoculum	Pigs	Sex	Age (weeks)	Weight (kg±SD)	Route	Dpi/ Analysis
A	RHDV-3A-VLP pulsed moDCs	3	M	6-7	20.5±2.8	SC	D14 Local and systemic responses
B	RHDV-VLP pulsed moDCs	3	M	6-7	18±1	SC	D14 Local and systemic responses
C	Medium	2	M	6-7	19.3±0.4	SC	D14 Local and systemic responses
D	Un-pulsed moDCs	2	M	6-7	18.8±1.8	SC	D14 Local and systemic responses
E	SPIO-moDCs	2*	F	4-5	12.2±0.8	SC	D2 MRI and Perls
F	RHDV-3A-VLP pulsed SPIO-moDCs	2*	F	4-5	13.4±1.1	SC	D7 Local and systemic responses, Perls

SC: subcutaneous injection; Dpi: days post immunization; Perls: Prussian Blue staining for iron particles. M: male; F: female. Weight represents the mean ± standard deviation of all animals in the group.
***** one animal was inoculated with 25 µg Fe/ml and the other with 50 µG Fe/ml of SPIO.

Tabla 2. Histopathological score of superficial inguinal lymph nodes.

Animal	H-E	Perls
A1	+	NP
A2	-	NP
A3	+	NP
B1	+	NP
B2	-	NP
B3	-	NP
C1	-	-
C2	-	-
D1	-	-
D2	++	-
E1	-	0,27 (50)
E2	+	0,21 (25)
F1	-	3,53 (50)
F2	-	1,54 (25)

H-E. The reactivity of the InLNs was evaluated taking into account the percentage of secondary cortical follicles regarding the whole LN; the following scoring was used: 0-5% (-), 0-30% (+), 30-70% (++), 70-100% (+++). **Perls**: The amount of positive cells was measured using digital morphometry software (ImageJ). Two sections were analyzed for each lymph node, and for each section, three low power fields (10x) were randomly selected. In each field, the percentage of area occupied by positive cells was calculated. The table expresses the average of these measures. (50 or 25) indicate the SPIO µg Fe/ml inoculated in the animal; (-) negative; NP: not performed.

Supplementary material for online publication only

Click here to download Supplementary material for online publication only: Crisci2014_Supp data_Fig. 7.tif

Supplementary material for online publication only

Click here to download Supplementary material for online publication only: Crisci2014_Supp Fig.8.tif